Lyman α emission from the first galaxies: signatures of accretion and infall in the presence of line trapping

Latif, M. A.; Schleicher, Dominik R. G.; Spaans, M.; Zaroubi, S.

Published in:
Monthly Notices of the Royal Astronomical Society

DOI:
10.1111/j.1745-3933.2011.01026.x

Publication date:
2011

Monthly Notices of the ROYAL ASTRONOMICAL SOCIETY LETTERS

Mon. Not. R. Astron. Soc. **413,** L33–L37 (2011) doi:10.1111/j.1745-3933.2011.01026.x

Lyman α emission from the first galaxies: signatures of accretion and infall in the presence of line trapping

M. A. Latif,[1⋆] Dominik R. G. Schleicher,[2,3] M. Spaans[1] and S. Zaroubi[1,4]

[1]*Kapteyn Astronomical Institute, University of Groningen, PO Box 800, 9700 AV Groningen, the Netherlands*
[2]*Leiden Observatory, Leiden University, PO Box 9513, NL-2300 RA Leiden, the Netherlands*
[3]*ESO Garching, Karl-Schwarzchild-Str.2, 85748 Garching bei Munchen, Germany*
[4]*Physics Department, Technion, Haifa 32000, Israel*

Accepted 2011 February 1. Received 2011 January 25; in original form 2010 December 9

ABSTRACT

The formation of the first galaxies is accompanied by large accretion flows and virialization shocks, during which the gas is shock heated to temperatures of $\sim 10^4$ K, leading to potentially strong fluxes in the Lyman α line. Indeed, a number of Lyman α blobs have been detected at high redshift. In this Letter, we explore the origin of such Lyman α emission using cosmological hydrodynamical simulations that include a detailed model of atomic hydrogen as a multi-level atom and the effects of line trapping with the adaptive mesh refinement code FLASH. We see that baryons fall into the centre of a halo through cold streams of gas, giving rise to a Lyman α luminosity of at least 10^{44} erg s^{-1} at $z = 4.7$, similar to the observed Lyman α blobs. We find that a Lyman α flux of 5.0×10^{-17} erg cm^{-2} s^{-1} emerges from the envelope of the halo rather than its centre, where the photons are efficiently trapped. Such emission can be probed in detail with the upcoming James Webb Space Telescope (JWST) and will constitute an important probe of gas infall and accretion.

Key words: methods: numerical – galaxies: formation – cosmology: theory – early Universe.

1 INTRODUCTION

Early-type galaxies are known to produce copious Lyman α photons due to their spatially extended gas distribution. In protogalactic haloes gas transfers its gravitational binding energy to the excitation of hydrogen atoms which results in Lyman α emission (Haiman, Spaans & Quataert 2000; Dijkstra, Haiman & Spaans 2006a,b). Therefore, the gas in dark matter haloes exceeding a virial temperature of $\sim 10^4$ K may be detected in the Lyman α line emission. The presence of ionizing radiation sources may enhance the Lyman α flux as gas is photoionized, and supernova feedback may further increase the escape fraction by generating a more clumpy structure. These ionization sources could be the first stars or mini-quasars. A luminous quasar can boost the emission of Lyman α photons by several orders of magnitude (Haiman & Rees 2001).

Many Lyman α blobs (LABs) have been observed at high redshift (Steidel et al. 2000; Matsuda et al. 2004; Saito et al. 2006; Saito et al. 2008; Yang et al. 2009; Ouchi et al. 2009). In the light of recent detections at redshift >7 (Lehnert et al. 2010; Vanzella et al. 2010), it is of high interest to understand what drives the emission and how it is spatially distributed. A number of LABs have been observed whose most probable origin is cold accretion of gas on to dark matter haloes (Nilsson et al. 2006; Smith & Jarvis 2007).

Numerical simulations show that cooling by Lyman α radiation induces collapse in protogalactic haloes. Moreover, baryons accumulate into the centre of haloes by penetration of cold streams of gas through the shock-heated medium (Fardal et al. 2001; Wise, Turk & Abel 2008; Jappsen et al. 2009; Regan & Haehnelt 2009; Dekel et al. 2009; Kereš et al. 2009; Faucher-Giguère et at. 2010; Goerdt et al. 2010; Shang, Bryan & Haiman 2010; Latif, Zaroubi & Spaans 2011). Cold streams with temperatures of $\sim 10^4$ K could be potential sources of spatially extended Lyman α emission (Dijkstra & Loeb 2009). Johnson et al. (2010) found that Lyman α radiation can also be emitted during accretion of gas on black holes formed by direct collapse in the first galaxies. Such emission is potentially detectable with James Webb Space Telescope (JWST).[1] Similarly, it allows to probe the starburst component through the enhanced emission in several recombination lines (Johnson et al. 2009).

The presence of large columns of neutral hydrogen gas causes the trapping of Lyman α photons (Spaans & Silk 2006; Latif, Zaroubi & Spaans 2011; Schleicher, Spaans & Glover 2010), which was neglected in some of the previous studies. In this Letter, we aim at a self-consistent modelling of Lyman α emission driven by accretion flows, including dynamics, non-equilibrium chemistry of H, H^+, He, He^+ and He^{++}, detailed level populations of atomic hydrogen, as well as the trapping of hydrogen line photons due to large column

⋆E-mail: latife@astro.rug.nl

[1] http://www.stsci.edu/jwst/instruments/nirspec/sensitivity

densities. The prime objective of this work is to study the origin and spatial distribution of Lyman α emission, which is detectable with JWST.

2 MODELLING OF THE PHYSICS

For our simulations, we employ an extended version of the adaptive mesh refinement (AMR) hydrodynamics code FLASH (Dubey et al. 2009). FLASH is a module-based Eulerian grid parallel simulations code. We use an AMR grid to achieve high dynamic resolution in the regions of interest. We employ the directionally split piece wise parabolic method (PPM) for hydrodynamic calculations, which is an improved form of the Godunov method (Colella & Woodward 1984). This method is well suited for flows involving shocks and contact discontinuities. The dark matter is simulated based on the particle mesh (PM) method. In order to create Gaussian random field initial conditions, we run the COSMICS package developed by Bertschinger (1995). We start our simulation at redshift 100. Our computational periodic box has a comoving size of 10 Mpc. We perform our simulations in accordance with the Λ cold dark matter model with *Wilkinson Microwave Anisotropy Probe* 5-years parameters. We select a $4 \times 10^9\,\mathrm{M}_\odot$ halo at redshift 7 and follow its collapse. We enforce eight additional levels of refinement, which gives 15 levels of refinement in total. In this way, we obtain a dynamic resolution limit of 70 pc (comoving), and can still follow the further evolution until redshift $z = 4.7$. We impose the Truelove criterion by refining according to the Jeans length (Truelove et al. 1997). We resolve the Jeans length by at least 20 cells. Such resolution was shown to be sufficient for accurately resolving turbulent structures during gravitational collapse (Federrath et al. 2010). When the highest refinement level is reached, we prevent artificial fragmentation via Jeans heating. We assume a primordial gas composition with 75 per cent hydrogen and 25 per cent helium by mass.

We have developed a chemical network for the non-equilibrium modelling of non-molecular species. For this purpose, we solve the rate equations of the following species $\mathrm{H}, \mathrm{H}^+, \mathrm{He}, \mathrm{He}^+, \mathrm{He}^{++}$ and e^- for non-equilibrium ionization. The rate equations for these species are solved using the backward difference formula (BDF) method of Anninos et al. (1997). We adopt the chemical rates of Abel et al. (1997) and Schleicher et al. (2008). We further solve for the level populations of atomic hydrogen up to the fifth electronically excited state, and model the non-equilibrium cooling including hydrogen line emission, collisional ionization cooling, recombination cooling, bremsstrahlung cooling and Compton cooling/heating. The transition rates for the level populations are based on the work of Omukai (2001). At an optical depth $\tau_0 > 10^7$, the photon escape time becomes longer than the gas free-fall time. Because of the weak dependence of the photon escape time on the gas number density, $t_{\rm ph} \propto n^{-1/9}$, trapping becomes important during the collapse since the latter scales as $n^{-1/2}$. A detailed discussion of such line trapping effects is given by Omukai (2001), Spaans & Silk (2006) and Schleicher et al. (2010). We have computed the Lyman α luminosity by determining the Lyman α emissivity and integrating it over the virial volume of a halo. Further details of the luminosity and flux calculation can be found in Dijkstra et al. (2006a).

3 RESULTS AND CONCLUSIONS

The initial density perturbations decouple from the Hubble flow and begin to collapse via gravitational instabilities. The gas is shock heated during the non-linear collapse of density perturbations. At redshift 10, the halo begins to virialize. In the process of virialization, part of its gravitational energy is converted into thermal energy. This heats up the gas and results in the emission of Lyman α photons. The gas is accreted into the centre of the halo through cold streams of $\sim 10^4$ K as shown in Fig. 1. The upper panels of Fig. 1 show the density at different redshifts while lower panels show corresponding temperatures. Typical number densities of the cold streams are of the order of 0.01–1 cm^{-3}. Density and temperature radial profiles are depicted in the upper-left and right-hand panels of Fig. 2. We see that in the presence of hydrogen line emission the gas cools isothermally. The density profile of the halo is $\sim r^{-2.3}$, which agrees with the results of Wise et al. (2008). The ionization degree of the gas is shown in the bottom-left panel (H II abundance) of Fig. 2. We see that most of the gas remains neutral at 10^4 K, and ionized fraction goes down due to faster recombination at higher densities $\sim n^{-0.5}$. The gas radial velocity is depicted in the bottom-right panel of Fig. 2. It can be seen from the figure that gas is falling into the centre of the halo. The velocity profile also shows that gas is accreted on to the halo through accretion shocks. The cold streams have typical column densities of about $10^{19}\,\mathrm{cm}^{-2}$. A radial profile of the column density is shown in Fig. 3. At columns above $10^{21}\,\mathrm{cm}^{-2}$ the gas optical depth exceeds 10^7 and Lyman α trapping becomes effective. The Lyman α emissivity is shown in Fig. 3. It can be seen from the figure that above columns of the order of $10^{22}\,\mathrm{cm}^{-2}$, Lyman α photons are trapped and cooling through this line is completely suppressed. That is why the Lyman α emissivity sharply declines in Fig. 3. We explored the local density variations and found that the maximum variation of the column density does not exceed an order of magnitude. In this sense, our calculation should provide a conservative lower limit on the expected flux. In the presence of Lyman α trapping, cooling can proceed through higher electronic states of atomic hydrogen (Schleicher et al. 2010). For comparison, the total emissivity from higher states of atomic hydrogen and recombination/bremsstrahlung processes is shown in Fig. 3. The total emissivity plot shows that despite line trapping, cooling still proceeds through these higher states of atomic hydrogen, particularly through 2s–1s and 3–2 transitions, and the thermal evolution is approximately isothermal.

The radial profile of the enclosed Lyman α luminosity is shown in Fig. 3. If the emission originates preferentially from the centre, an approximately flat profile would be expected, while for uniform emission, a power-law behaviour as $\sim r^3$ would be expected due to volume effects. Here, we find the absence of emission in the central core, and then a sharp increase in luminosity between radii of $10^{20.2}$ and 10^{21} cm by four orders of magnitude, and a more modest increase between radii of 10^{21} and 10^{22} cm. This behaviour reflects the generation of Lyman α emission through accretion shocks. JWST can confirm the presence of such a brightness profile. The total Lyman α luminosity from the halo is $10^{44}\,\mathrm{erg\,s}^{-1}$, which is consistent with observed LABs (Ouchi et al. 2009; Goerdt et al. 2010).

The emerging flux from the halo is depicted in Fig. 3. We find a total flux of $5.0 \times 10^{-17}\,\mathrm{erg\,cm}^{-2}\,\mathrm{s}^{-1}$. At redshift 4.7, the observed Lyman α wavelength is at 0.68 μm. This can be detected with the JWST-instrument NIRSpec for integration times of 10^4 s, with S/N = 10 and $R = 100$. JWST spectrograph NIRSpec will have angular resolution of 0.1 arcsec for 2 μm, and NIRcam will be well suited for higher angular resolution with field of view of $2.2 \times 2.2\,\mathrm{arcmin}^2$ and 4096^2 pixels for shorter wavelength of 0.6–2.3 μm. The halo in our case will have an angular size of 0.5 arcsec at redshift 4.7. It should be detectable with NIRcam/NIRSpec. For extended emission of Lyman α, it may need higher integration time ($\sim 10^5$ s) to resolve the flux from extended sources. The total mass of our halo at

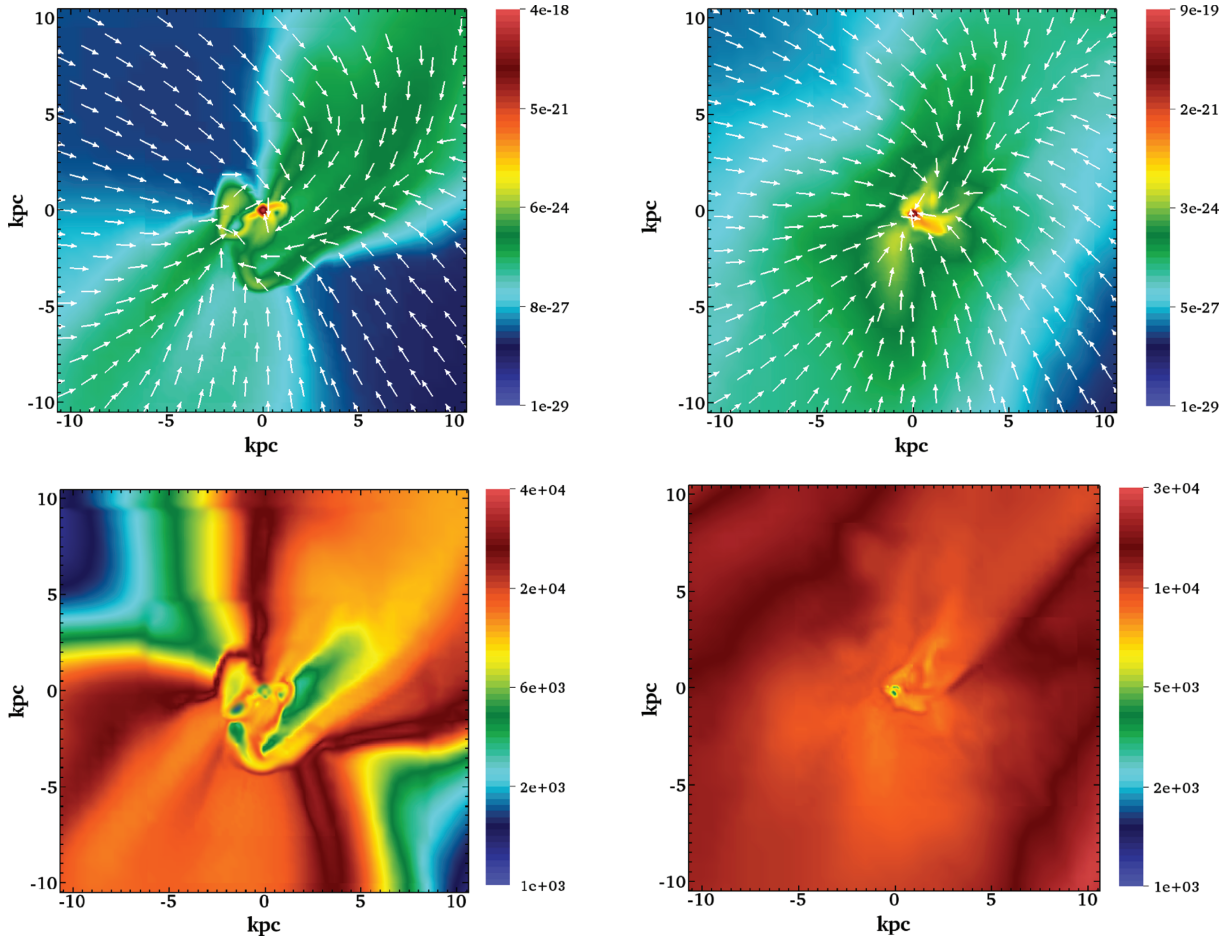

Figure 1. The upper panels show the density slices through the centre of the halo. The left-hand panel is for redshift 4.7 and right-hand panel for redshift 8. Velocity vectors are overplotted on the density slices. The bottom two panels show the corresponding temperatures. The figure shows the inner region of 20 kpc in comoving units.

redshift 4.7 is 2×10^{10} $M_{\odot}$, which is not extreme in any way. Selecting higher mass haloes will produce higher fluxes as there is a power-law relation between the mass of a halo and its luminosity $L_{\mathrm{Ly}\alpha} \propto M^{5/3}$ (Dijkstra et al. 2006a; Dekel et al. 2009). We stopped our simulation at a redshift of 4.7 as it becomes computationally too expensive to follow the further time evolution.

In this work, we assume that there is no X-ray/UV background flux. Its presence can heat the gas and may increase the Lyman α flux (Zaroubi et al. 2007; Spaans & Meijerink 2008). We have compared our results with Dijkstra et al. (2006a) and found good agreement. We have assumed here that the halo is metal free. The addition of small amounts of dust can absorb Lyman α photons efficiently, unless the gas is inhomogeneous (Haiman & Spaans 1999). However, in-falling gas may still be pristine for isolated haloes. We have ignored H_2 cooling, which is suppressed in the presence of a strong UV background ($J_{21} > 100$) (Dijkstra et al. 2004; Cazaux & Spaans 2009). Shang et al. (2010) found that even $J_{21} \sim 30$ will be sufficient to quench H_2 formation for local variations in flux (see Dijkstra et al. 2008). At higher redshifts, it is possible that H_2 may form for more modest radiation backgrounds. Even then, we expect H_2 formation preferentially at the centre of the halo, while the accretion at the virial radius may still include a gas phase at 10^4 K. This supports our main conclusion that Lyman α radiation originates mostly from gas in halo envelope.

Some LABs are also associated with massive star-forming galaxies (Matsuda et al. 2006) where stellar feedback or an active galactic nucleus (AGN) could power Lyman α radiation. It is clear that starbursts and AGNs are also potential candidates to power or enhance the observed Lyman α luminosities. It is not fully clear if our results are also applicable to such situations, although we expect similar effects of line trapping in the centres of such galaxies if $N_{\mathrm{H}}/\Delta v \geq 10^{21}$ cm^{-2} km^{-1} s, with Δv the cumulative velocity difference along the atomic hydrogen column N_{H}.Current modelling uncertainties concern both the star formation efficiency and the initial mass function. Both radiative feedback, leading to the formation of H II regions, and mechanical feedback, providing a more clumpy structure with higher escape fractions, need to be modelled self-consistently. Outflows if present may enhance the detectability of Lyman α emission in the outskirt of the halo; 5 per cent of the emitted Lyman α photons could be directly transmitted to the observer along the line of sight (Dijkstra & Wyithe 2010). In the future, cosmological radiative transfer simulations including feedback effects should be performed to obtain more robust results.

ACKNOWLEDGMENTS

The FLASH code was in part developed by the DOE-supported Alliance Center for Astrophysical Thermonuclear Flashes (ACS) at

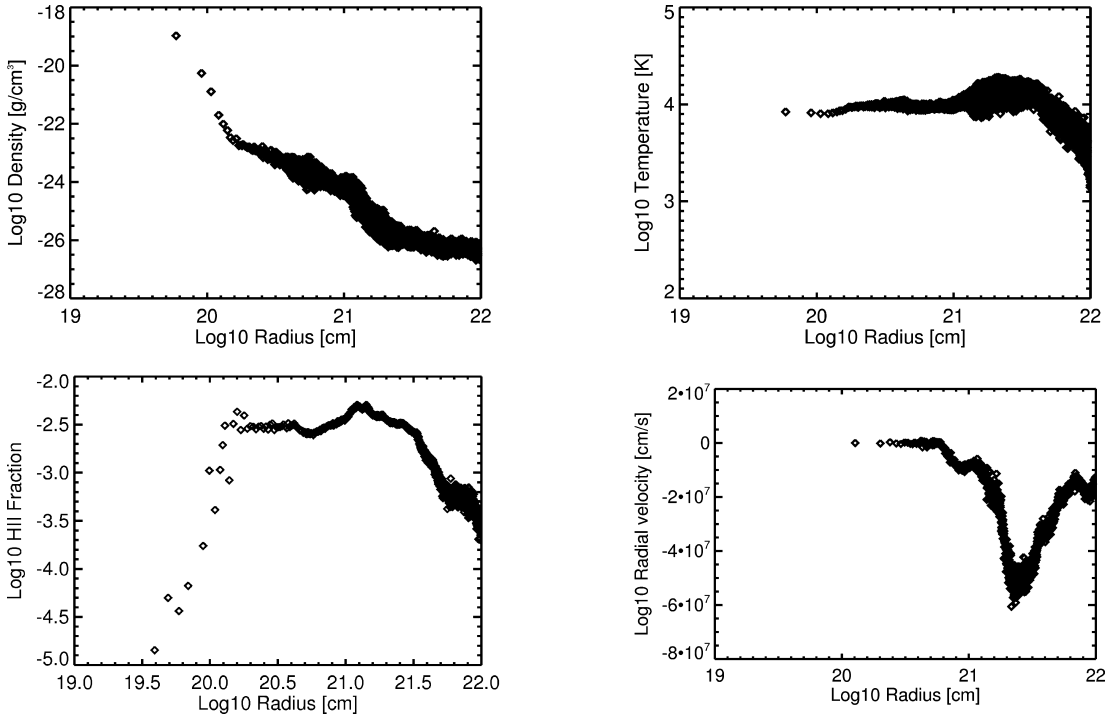

Figure 2. All panels are log–log plots. The upper-left panel shows the radial density profile of the halo. The radial temperature profile for the halo is depicted in the upper-right panel. H II abundance is shown in the lower-left panel. The radial velocity of the halo is depicted in the lower-right panel.

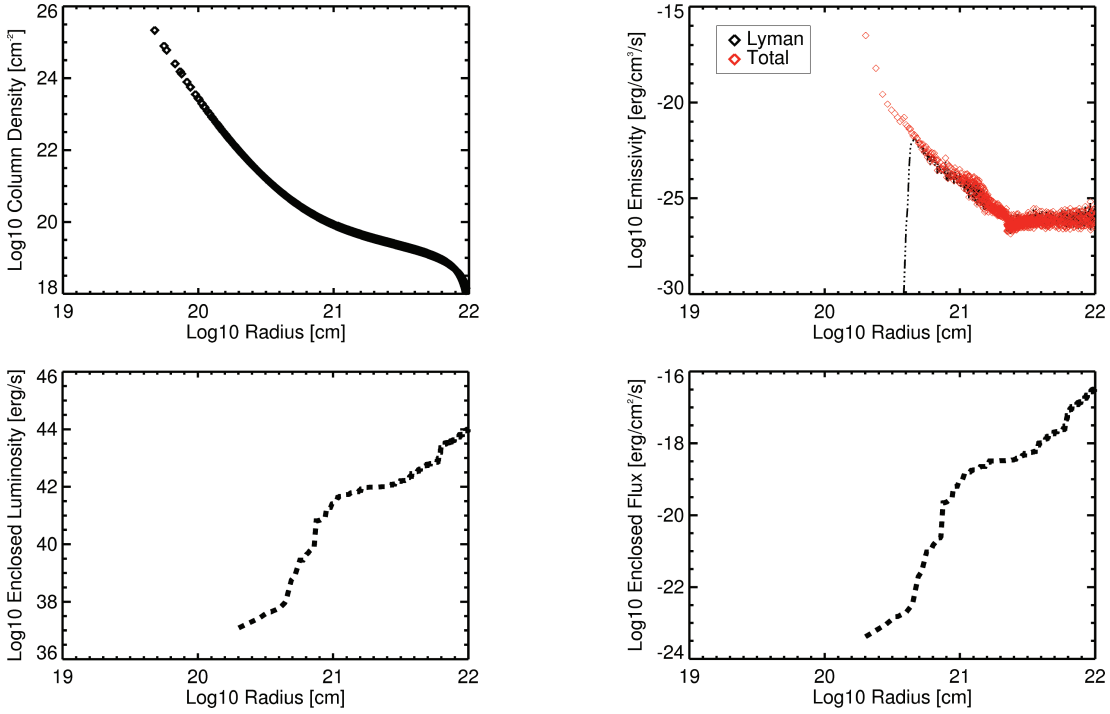

Figure 3. All panels are log–log plots. The upper-left panel shows column density plotted against the radius of the halo. Lyman α emissivity radial profile emerging from the halo is shown in the upper-right panel. Lyman α luminosity is shown in the lower-left panel. Lyman α flux is plotted against the radius of the halo in the lower-right panel.

the University of Chicago. DRGS acknowledges funding via the European Community Seventh Framework Programme (FP7/2007-2013) under grant agreement No. 229517 and via HPC-EUROPA2 (project number: 228398) with the support of the European Commission Capacities Area Research Infrastructures Initiative. SZ thanks the Lady Davis foundation for support. We thank the anonymous referee for a careful reading of the manuscript and many insightful comments.

REFERENCES

Abel T., Anninos P., Zhang Y., Norman M. L., 1997, Nat, 2, 181
Anninos P., Zhang Y., Abel T., Norman M. L., 1997, Nat, 2, 209
Bertschinger E., 1995, preprint (arXiv:astro-ph/9503125)
Cazaux S., Spaans M., 2009, A&A, 496, 365
Colella P., Woodward P. R., 1984, J. Comput. Phys., 54, 174
Dekel A. et al., 2009, Nat, 457, 451
Dijkstra M., Loeb A., 2009, MNRAS, 400, 1109
Dijkstra M., Wyithe J. S. B., 2010, MNRAS, 408, 352
Dijkstra M., Haiman Z., Rees M. J., Weinberg D. H., 2004, ApJ, 601, 666
Dijkstra M., Haiman Z., Spaans M., 2006a, ApJ, 649, 14
Dijkstra M., Haiman Z., Spaans M., 2006b, ApJ, 649, 37
Dijkstra M., Haiman Z., Mesinger A., Wyithe J. S. B., 2008, MNRAS, 391, 1961
Dubey A. et al., 2009, Parallel Comput., 35, 512
Fardal M. A. et al., 2001, ApJ, 562, 605
Faucher-Giguère C. A., Kereš D., Dijkstra M., Hernquist L., Zaldarriaga M., 2010, ApJ, 725, 633
Federrath C., Sur S., Schleicher D., Banerjee R., Klessen R. S., 2011, ApJ, in press (arXiv:1102.0266)
Goerdt T. et al., 2010, MNRAS, 407, 613
Haiman Z., Rees M. J., 2001, ApJ, 556, 87
Haiman Z., Spaans M., 1999, ApJ, 518, 138
Haiman Z., Spaans M., Quataert E., 2000, ApJ, 537, L5
Jappsen A., Klessen R. S., Glover S. C. O., Mac Low M., 2009, ApJ, 696, 1065
Johnson J. L. et al., 2009, MNRAS, 399, 37
Johnson J. L., Khochfar S., Greif T. H., Durier F., 2010, MNRAS, 410, 1427
Kereš D. et al., 2009, MNRAS, 395, 160
Latif M. A., Zaroubi S., Spaans M., 2011, MNRAS, 411, 1659
Lehnert M. D. et al., 2010, Nat, 467, 940
Matsuda Y. et al., 2004, AJ, 128, 569
Matsuda Y. et al., 2006, ApJ, 640, L123
Nilsson K. K. et al., 2006, A&A, 452, L23
Omukai K., 2001, ApJ, 546, 635
Ouchi M. et al., 2009, ApJ, 696, 1164
Regan J. A., Haehnelt M. G., 2009, MNRAS, 396, 343
Saito T., Shimasaku K., Okamura S., Ouchi M., Akiyama M., Yoshida M., 2006, ApJ, 648, 54
Saito T., Shimasaku K., Okamura S., Ouchi M., Akiyama M., Yoshida M., Ueda Y., 2008, ApJ, 675, 1076
Schleicher D. R. G. et al., 2008, A&A, 490, 521
Schleicher D. R. G., Spaans M., Glover S. C. O., 2010, ApJ, 712, L69
Shang C., Bryan G. L., Haiman Z., 2010, MNRAS, 402, 1249
Smith D. J. B., Jarvis M. J., 2007, MNRAS, 378, L49
Spaans M., Meijerink R., 2008, ApJ, 678, L5
Spaans M., Silk J., 2006, ApJ, 652, 902
Steidel C. C. et al., 2000, ApJ, 532, 170
Truelove J. K. et al., 1997, ApJ, 489, L179
Vanzella E. et al., 2010, ApJ, preprint (arXiv:1011.5500)
Wise J. H., Turk M. J., Abel T., 2008, ApJ, 682, 745
Yang Y. et al., 2009, ApJ, 693, 1579
Zaroubi S., Thomas R. M., Sugiyama N., Silk J., 2007, MNRAS, 375, 1269

This paper has been typeset from a TEX/LATEX file prepared by the author.